Biofilm growth on rugose surfaces[*]

D. Rodriguez

Departamento de Matemática Aplicada,

Universidad Complutense de Madrid; Madrid, Spain

B. Einarsson

Center for Complex and Nonlinear Science,

University of California at Santa Barbara; California, USA

A. Carpio

Departamento de Matemática Aplicada,

Universidad Complutense de Madrid; Madrid, Spain, and

School of Engineering and Applied Sciences,

Harvard University; Cambridge, Massachusetts, USA

(Dated: January 25, 2013)

Abstract

A stochastic model is used to assess the effect of external parameters on the development of submerged biofilms on smooth and rough surfaces. The model includes basic cellular mechanisms, such as division and spreading, together with an elementary description of the interaction with the surrounding flow and probabilistic rules for EPS matrix generation, cell decay and adhesion. Insight on the interplay of competing mechanisms as the flow or the nutrient concentration change is gained. Erosion and growth processes combined produce biofilm structures moving downstream. A rich variety of patterns are generated: shrinking biofilms, patches, ripple-like structures traveling downstream, fingers, mounds, streamer-like patterns, flat layers, porous and dendritic structures. The observed regimes depend on the carbon source and the type of bacteria.

PACS numbers: 87.10.Mn,87.18.Hf,87.85.M

I. INTRODUCTION

Many bacterial species adapt to hostile environments forming aggregates called biofilms. Formation of bacterial biofilms on solid surfaces in aqueous environments is a collective effect of great importance in medicine and engineering. In such environments, bacteria may attach themselves to a solid surface and to each other by mechanisms that need clarification, produce extracellular polymeric substances (EPS) and change their morphology [1]. The result is the formation of a film on the solid surfaces that contains live bacteria, grows on a wide range of hydrated supports, e.g. tissue, plastic, metal, rocks, etc, and is extremely resistant to external aggressions due to antibiotics, chemicals or flows. Once formed, biofilms may grow, expel cells and film fragments that are carried by the flow and may in turn reattach themselves to other solid surfaces colonizing them [1].

Biofilms are responsible for a large percentage of infections in humans, ranging from deadly illnesses, e.g. cystic fibrosis and legionellosis, to life threatening infections originated at artificial joints, pacemakers or catheters [2–4]. Biofilm induced damage causes substantial economic losses, due to biocorrosion of aircraft fuselages or metallic structures, biofouling of ship hulls, efficiency reduction in heat exchange-systems, pressure drop and clogs in water systems, food and water poisoning [5], and so on. On the other hand, bioremediation seems to be one of the fastest growing fields nowadays. Some bacterial strains feed on a wide variety of toxic pollutants. Such microorganisms may be deliberately released to clean up oil spills or to purify underground water in farming land and mines [4]. At the same time, the development of synthetic biology is paving the way for the use of biofilms as biosensors or bioindicators for monitoring the presence of certain chemicals in the environment [6–12]. Attempts to engineer devices out of biofilms continue to take place. Electrooptical devices have already been created [13]. There are efforts to use biofilms emitting optic signals as microsensors in microdevices. To indicate correctly the order of magnitude of any variable on the walls they attach to, biofilms should be kept thin and homogeneous. Pattern formation should be avoided. If we are to control biofilms grown on specific parts of a device, such surfaces must have well defined properties. In particular, a defined roughness pattern. Standardized manufacturing of substrates is necessary to ensure similar biofilm quality under analogous external conditions. Surfaces with an unknown microstructure are mechanically processed by means of milling machines before being used as substrates. The

resulting roughness, determined by the milling cutters, is typically of the same order of magnitude as the size of the bacteria. Therefore, the effect of such roughness patterns on biofilm growth under different flow conditions must be accounted for.

Understanding biofilm development and their response to changes in the environment is essential to controlling them in engineering and medical systems, either to destroy them when unwanted, or to better exploit them when beneficial. General models describing biofilm dynamics can be classified in three groups according to their description of bacteria [14–16]: continuum, individual based (IbM) or cellular automata (CA) models. Continuum models treat the biofilm as a material, typically a gel, polymer or viscous fluid [17–19]. They are often two-phase models comprising the fluid containing the nutrients and the biofilm [20]. When available, thin film approximations may be more effective [21]. In IbM models, microbes or clusters of microbes are seen as hard spherical particles or macroscopic objects with mechanical properties that evolve according to reaction-diffusion equations for nutrients and oxygen coupled with descriptions of bacterial growth and spreading of biomass [22]. Hybrid variants include the EPS matrix as an incompressible viscous flow, which embeds the discrete microbial cells [23]. Hybrid models combine discrete descriptions of the cells with continuous descriptions of other relevant fields [24, 25]. A hybrid model trying to account for the effect of the flow is proposed in [26]. CA models distribute biomass over a cellular grid and allow its cells to change with appropriate probabilities according to a set of simple rules [27, 28]. Available CA models already include a few bacterial mechanisms and activities in a reasonable way. However, the description of more complex mechanisms, such as microbe attachment to surfaces [29, 30], quorum sensing to form biofilms [31, 32], generation of EPS matrix [33–35] and interaction with the surrounding flow [36–38] remains unclear.

The most appropriate model for a particular biofilm should take into account the specific bacteria, the environment in which the biofilm is formed, the parameters that can be fitted to experiments, and the predictions to be made [14–16]. We have in mind understanding experiments of submerged biofilm growth in micropipes, on surfaces whose roughness is of the same order of magnitude as the bacterial size. Despite the vast amount of literature on biofilm modeling, we are not aware of previous attempts to include such roughness patterns in the models. The size of the bacteria being comparable to the magnitude of the roughness, we have chosen to borrow ideas from cellular automata strategies, conveniently modified to

3

account for surface roughness. To reduce the computational cost, we focus on a two dimensional reduction, though the three dimensional version of the model is discussed too. We reproduce qualitatively patterns and trends that remind of those observed in experiments, and are able to make a few additional predictions. However, additional processes like cell displacement within the biofilm or movement of biofilm blocks induced by external forces have yet to be included in the model for a better understanding of pattern formation processes. Experimental measurements of some parameters (unavailable at present) should be required to attempt quantitative comparisons. Fitting model parameters to practical set-ups seems to be a general problem with models for biofilms due to lack of adequate experimental data [15, 24].

The paper is organized as follows. Section 2 collects basic facts on biofilms and fixes the set-up for the problem, based on experiments of submerged biofilm growth. Section 3 presents a two dimensional model for aerobic biofilm growth in micropipes, together with the probabilistic rules for cellular division and spreading, detachment due to the flow, EPS matrix generation, decay and adhesion. We propose an asymmetric erosion mechanism adapted to flows moving parallel to the surface, together with simple probabilistic rules accounting for EPS matrix generation and its influence on biofilm cohesion. Section 4 extends the model to three dimensions. Section 5 focuses initially on the evolution of biofilm seeds already attached to the substratum for different nutrient concentrations and increasing ratios of the shear due flow to the biofilm cohesion. For large ratios, flat biofilm seeds are washed out on smooth surfaces in three dimensions, see Figure 10. As the ratio shear/cohesion is decreased or the nutrient concentration is increased, ripple-like and streamer-like patterns are generated, see Figures 11 and 12. Such ripples travel downstream with the current. Streamer-like patterns may detach when they surpass a certain size. For smaller ratios or larger concentrations, tower-like structures may develop, see Figure 14. The influence of the model parameters on the patterns is investigated in more detail by means of the two dimensional reduction. The evolution of the patterns with some parameters seems to follow qualitative trends experimentally observed, by other groups [36, 39–43] and by ourselves [44]. However, the effect of mechanical processes like displacement of cell aggregates due to external forces, thought to be relevant in the dynamics of real biofilm patterns such as streamers, must yet be accounted for. Biofilm evolution depends on the combinations of cell processes activated and a small set of parameters. The simulations provide some

4

insight on the effect of competing mechanisms. Erosion and growth alone are able to produce biofilm structures moving downstream. The regimes observed as the flow varies are influenced by the carbon source, the type of bacteria and the nutrient concentration. This may lead to flatter biofilms or enhanced pattern formation. When the current is strong enough compared to the biofilm cohesion, biofilm seeds seem to evolve into thin flat biofilms for most nutrients, which may break into patches and tend to be washed out on smooth surfaces but may be stabilized by some choices of surface roughness. Numerical simulations suggest that roughness of a slightly larger size than the bacterial size may enhance biofilm ability to survive and cover surfaces in a more uniform way, see Figures 15-17 and 20. Other types of roughness may hinder biofilm growth. Adhesion of floating cells on uncolonized surfaces may produce patchy configurations at low adhesion rates, that may become wavy biofilm layers at larger adhesion rates. Finally, Section 6 discusses our conclusions and perspectives for future work.

II.   BIOFILM STRUCTURE AND EXPERIMENTS OF PATTERN FORMATION

Biofilms are a survival strategy developed to create homeostatic conditions which favor bacterial survival in hostile environments. The first scientific evidence of biofilm existence is due to Antonie Van Leeuwenhoek in 1680, who detected these structures while studying the dental plaque. In 1978, William Costerton isolated bacterial cells in completely different bacterial developments from those suspended or "planktonic" cells seen until that year in laboratories. He named them biofilms [45]. Until then, the same bacterial strain was used during several generations, keeping it in optimal growth conditions. This induces the natural genetic selection of bacteria unable to generate biofilms, which are a natural mechanism to survive in adverse environments.

Biofilms can be defined as a large amount of microcolonies embedded inside a polysaccharid matrix attached to a solid surface in an aqueous environment. This matrix offers numerous advantages: it gives increased resistance against external aggressions, such as chemicals, high shear flows, radiation, etc., it can be used as a food reservoir, and creates a suitable environment to reproduce [46]. The external medium provides the substances bacteria need to live. Figure 1 shows biofilm patches formed by bacteria genetically modified by inserting the gene for the production of green fluorescent protein (GFP). This protein
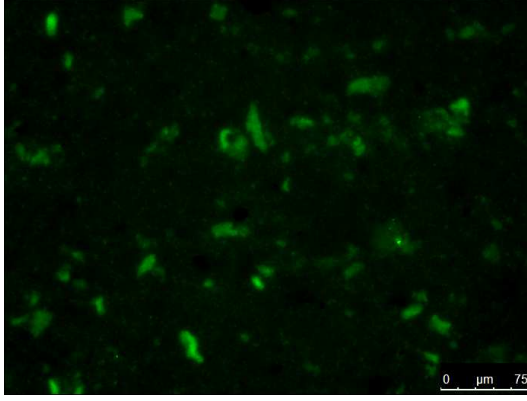
FIG. 1. Biofilm patches formed by Pseudomonas putida on a polycarbonate substratum at $Re = 100$. Image taken with a confocal LEICA SP5 fluorescence microscope.

becomes fluorescent when exposed to light, allowing to locate the biofilm fragments attached to the surface.

Since Costerton's work, the field has developed continuously [1, 4, 19, 33, 34, 47–52]. However, many issues concerning biofilm behavior and its responses to changes in the environment remain unresolved. The life cycle of biofilms has been largely studied [1, 53]. The main developmental stages are: colonization, growth, spread, maturation and death. A scheme of a submerged biofilm life cycle is shown in Figure 2. Different bacterial species may create different types of biofilms depending on the growth conditions. Biofilms may stick on air/solid or air/liquid interfaces [50] forming wrinkled films. We consider here submerged biofilms attached to solid surfaces surrounded by a flow, formed by aerobic bacteria.

The colonization of new surfaces is a critical stage of the biofilm development. Bacteria have the ability to detect concentration gradients (which are related to the presence of a surface) [30, 47]. Microorganisms use cilia or flagella to reach the surface, trying to attach to it. The attachment process induces several changes in the morphology of bacteria and their behavior, marking the onset of the development of a biofilm: loss of flagella or cilia, changes in cell phenotype and start of reproduction process to create a microcolony.

If aerobic bacteria receive sufficient amounts of carbon and oxygen, they divide and proliferate on the surface forming microcolonies that constitute the germ of a biofilm and may eventually merge. The metabolism of the cells near the biofilm surface restricts the diffusion of oxygen and carbon to bacteria at the bottom of the colony. A fraction of cells in the biofilm begin to produce exopolysaccharides, forming the EPS matrix. This promotes
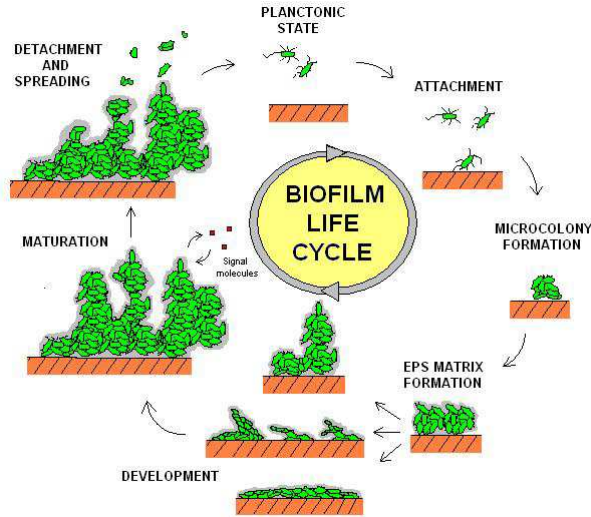
6

FIG. 2. Schematic development of a biofilm.

vertical growth of the colony, improves access to oxygen and carbon, and gives rise to a macrocolony [1, 35]. Cells therein are held together by a matrix that also contains dead cell debris and extracellular DNA. The surrounding flow subjects cells in the upper part of the colony to higher shear forces and these cells may be detached from the colony. External conditions modify its main characteristics, generating different internal and external structures optimized to improve nutrient obtention and mechanical resistance to external shear stress. Typical macrocolonies consist of mushroom-like towers separated by fluid-filled voids carrying nutrients and oxygen, although flat structures are also possible. Depending on the hydrodynamic conditions, the nutrient availability, the nutrient source and the bacterial strain, circular colonies, streamers, ripples, rolls, streamlined patches or mushroom networks [36, 39] are observed, see Figure 3. A reversible evolution from one pattern regime to another by increasing or decreasing the nutrient concentration and the shear force has been observed experimentally in [43].

Once the biofilm has reached a certain thickness and its structure is well defined, quorum sensing processes activate the spread mechanism. This mechanism consists of a set of different strategies to release bacteria to the flow in order to colonize new surfaces and ensure the strain survival [39, 54]. Some examples are structure self weakening in the form of flow detachment or surface expansion produced by dragging mechanisms, like rippling, rolling or darting [1, 36]. Figure 3 illustrates some of these mechanisms.
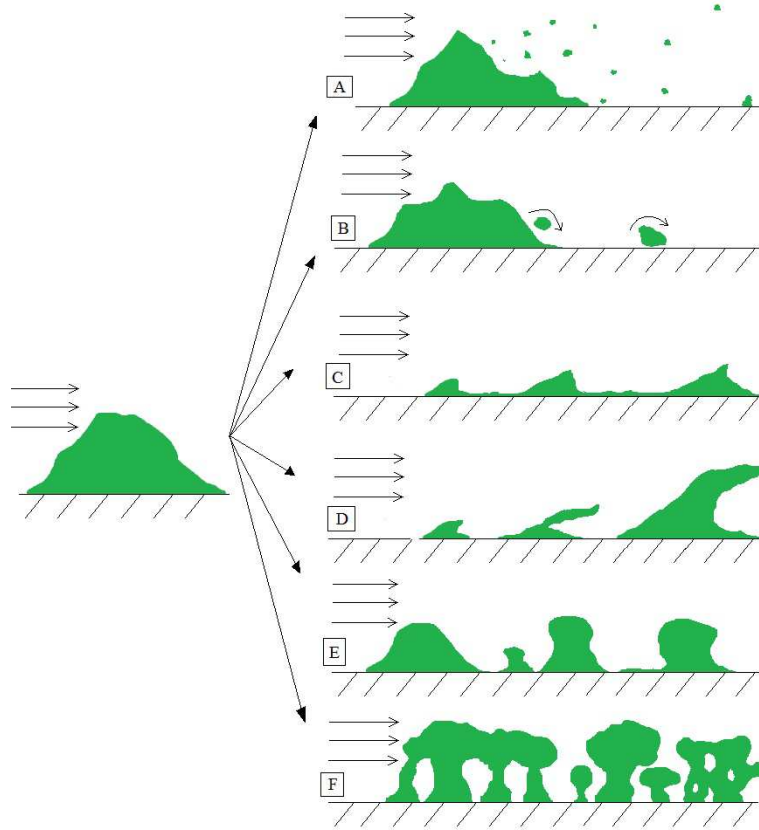
FIG. 3. Expansion and pattern formation mechanisms in submerged biofilms. (a) Darting: bacteria are expelled from the colony. (b) Rolling: bacterial clusters detach and roll over the surface. (c) Rippling: ridges and valleys form on the biofilm surface and may travel downstream. (d) Streamers: fingers curved in the direction of the flow. (d) Mounds: groups of hills. (e) Mushroom networks: mushroom-like towers grow and merge creating a porous structure with channels.

If the nutrient or oxygen concentration is not enough to sustain the population, cells start dying until an equilibrium between deaths, availability of nutrients, cellular growth and spread is reached.

Series of experiments (see [36] and [39–43], for instance) were performed to assess the influence of hydrodynamic conditions and nutrients on biofilm structure for specific bacterial strains. Experiments were made in rectangular glass flow cells with sections of a few millimeters. We summarize a few conclusions that will be kept in mind in the sequel. The EPS matrix was shown to determine biofilm cohesive strength. The shear force created as the fluid flows over its surface seemed to be the principal physical force acting on the
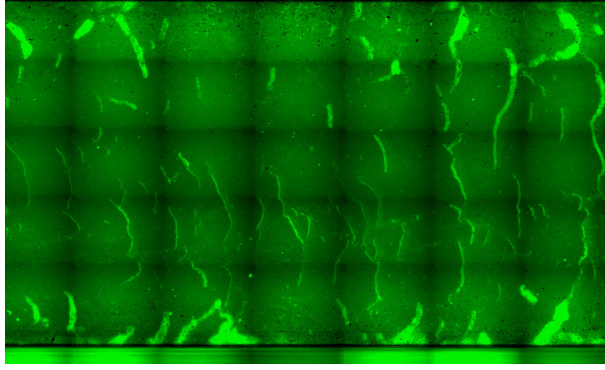
FIG. 4. Panoramic view of ripples formed by Pseudomonas putida on the bottom of a duct at $Re = 1000$, obtained by glueing together images taken along a grid.

biofilm. Biofilms grown under higher shear were observed to adhere more strongly and have a stronger EPS matrix than those created at low shear. Increasing the velocity of the fluid, biofilms created at lower Reynolds numbers were washed out. At low shear, detachment takes the form of sloughing. For higher shear forces, detachment occurs in the form of erosion, producing smoother, flatter and thinner biofilms. Mounds, ripples and streamers were identified. As the Reynolds number grew, round biofilm patches elongated with the current. The drag seemed to push newborn cells downstream. While ripples migrated downstream sliding over lower layers of biofilm without detaching, streamers seemed to be anchored. Ripples were observed in laminar and turbulent flows. Streamers were believed to appear in turbulent regimes. Recent experiments carried out in curved pipes with sections of a few hundred microns [55] have produced streamers in laminar flows, raising new issues about the mechanisms leading to streamer and pattern formation in submerged biofilms.

Additional experiments in rectangular flow cells, but on polycarbonate surfaces, consider the influence of roughness [44]. Comparing biofilm grown on standard surfaces and milled surfaces with an average roughness about $2 - 4\ \mu$m (slightly larger than the size of bacteria), more biofilm was observed to accumulate on the milled surface. Increasing the Reynolds number, almost no biofilm accumulated on the untreated surface. Patches, uniform covers with mounds, and ripples were identified on the milled surface as the Reynolds number was increased, see Figures 1 and 4. The experiments suggested that the specific roughness pattern selected might enhance biofilm formation and expansion.
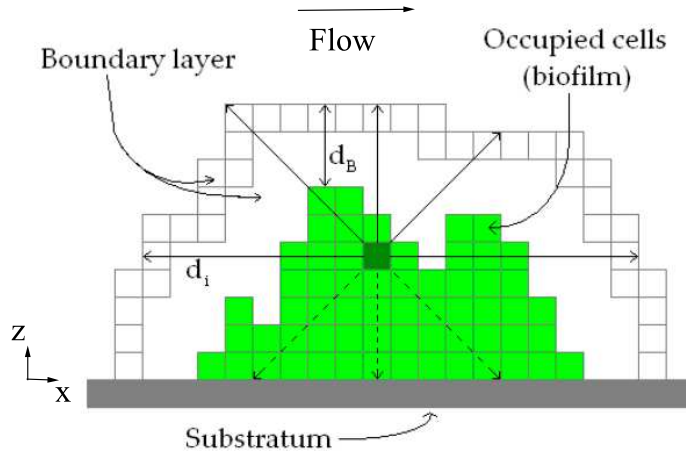
9

FIG. 5. Geometry for the cellular automata description.

III. TWO DIMENSIONAL MODEL

In line with the experiments described at the end of the previous section, the geometry selected for our model is a rectangular duct with a rough bottom surface. The roughness has the same order of magnitude as the bacterial size. An aqueous solution containing nutrients flows along the pipe in the x direction. We take a longitudinal section of the rectangular pipe (x=length, z=height) and study biofilm evolution in it, see Figure 5. Next section extends the model to three dimensions.

We consider bacteria as living entities that may perform a certain number of activities depending on external factors. They may divide and spread, generate EPS matrix, deactivate, detach from the biofilm and so on. Aerobic bacteria need oxygen and a carbon source to survive. Bacteria choose to carry out one activity or another with a certain probability according to the levels of nutrient and oxygen available at its location and the shear force exerted by the flow. This point of view makes it easier to incorporate the interaction with roughness patterns. In most simulations, biofilms will be grown from an initial seed that is already attached to the substratum. We will allow for adhesion of floating cells at the end.

In a CA model, space is represented by a grid of square tiles, see [27, 28] and references therein. In view of our roughness patterns, we choose the size of the tiles a to be similar to the size of one bacterium (microns) [56]. Notice that we envisage tubes with sizes of a few hundred microns. Each tile is filled with either one bacterium, water or bottom surface material, and its status may change from one time step to the next according to the rules
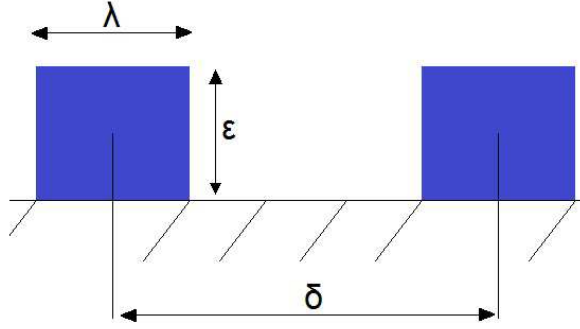
FIG. 6. Roughness pattern.

governing the different processes. Each individual bacteria evolves according to the nutrient and oxygen presence it feels, to its affinity to the carbon source, to the flow strength it feels and to its location in the biofilm. Roughness is modeled by rectangular steps on the bottom, characterized by their height ϵ, the length of the peaks λ, and the distance between them δ, see Figure 6.

We propose a modular CA model organized in sub-models that depend on the aspects of biofilm formation and evolution we want to describe. Each sub-model deals with a distinctive bacterial mechanism: cellular division and spreading to neighboring tiles, generation of EPS matrix and decay, cell detachment and adhesion. For each individual bacteria each of these events will be assigned a probability that usually depends on the concentration of oxygen and nutrients, the fluid flow, the biofilm cohesion or the number of neighboring cells containing biomass and their location. We have chosen to cover the following aspects of biofilm formation and evolution:

- Dynamics of dissolved components (nutrients, oxygen) outside the biofilm and inside. Experiments are usually designed in such a way that their concentrations are almost constant outside the biofilm. Inside, they are governed by reaction-diffusion equations, but a quasi-steady approximation thereof might suffice because the diffusion and reaction of dissolved components are likely to be faster than the rates of biological processes [23, 37, 57].

- Detachment of isolated bacteria, biofilm erosion and detachment of biofilm fragments. Each cell has a probability to detach from the biofilm depending on its location, the number and location of neighboring bacteria, the force exerted by the flow and the

11

cohesion of the biofilm. Detached bacteria are carried by the flow. Biofilm fragments attached to the rest of the film by a few cells may also be eroded if the connection to the substratum breaks off.

- Generation of EPS matrix and decay. Each bacterium has a probability to produce EPS matrix depending on the flow and the concentration of substrate and oxygen [33–35]. The cohesion of the biofilm depends on the EPS matrix, which in turn affects mechanisms such as detachment [43]. Cell deactivation and decay mechanisms for low concentrations may generate inerts playing a role in biofilm adhesive properties.

- Reproduction and spreading. Each bacterium has a probability to reproduce depending on the availability of oxygen and nutrients. New bacteria fill neighboring empty tiles or shift existing bacteria with a certain probability.

- Adhesion of floating cells. The bacteria carried with the flow may attach either to existing biofilm parts or to uncolonized parts of the substratum with a certain probability that depends on the flow and the affinity between the bacterial strain and the surface [29, 30].

Selecting these basic mechanisms we are able to generate patterns and reproduce behaviors that remind of those observed in real biofilms. The true biological processes being yet largely unknown, the idea is to choose simple rules motivated by experimental observations trying to mimic some observed behaviors. Whenever a better understanding of the cellular processes is available, the proposed rules can be updated to reflect that knowledge. The selection of processes considered here provides insight on the role of different parameters in the structure of cellular aggregates, together with basic understanding of the way some competing cellular mechanisms may act and interact. This information might be incorporated in more refined models, or used for calibration to experiments. In our present model, the flow influences detachment and attachment processes, the concentration boundary layer outside the biofilm, and EPS matrix generation and cell reproduction through it. In our simulations, the biofilm/fluid interface moves, but as a result of erosion, adhesion, mass production and spreading. Depending on the shear force and the biofilm cohesion, the fluid might also move biofilm blocks or cells. A mechanism allowing external forces to shift cells is yet to be included.

We describe below our approach to incorporate the above mentioned mechanisms in each time step of the biofilm evolution.

A. Dissolved components

The evolution of an aerobic biofilm depends on the availability of carbon sources and oxygen. The concentrations of oxygen c_o and substrate c_s are governed by a convection-reaction-diffusion system. Since the diffusion and reaction of dissolved components are faster than the rates of biological processes [23, 37, 57], quasi-steady approximations suffice. Outside the biofilm, the concentrations follow uncoupled convection-diffusion equations. Inside the biofilm, the convection due to the flow disappears, but coupling reaction terms representing nutrient and oxygen uptake by cells must be included. The model is completed with boundary conditions at the walls of the duct and the bulk/boundary layer interface [37]. Experiments are usually designed to keep concentrations almost constant within the bulk fluid. Nutrient concentration gradients result from a combination of nutrient transport from the bulk fluid through a concentration boundary layer adjacent to the biofilm/fluid interface and nutrient uptake uptake by the cells. The thickness of the concentration boundary layer characterizes the external mass transport and depends on the flow regime. Experimental measurements of the nutrient concentration gradients and the boundary layer thickness for different flows are performed in [58, 59]. The thickness d_B was shown to depend on the bulk velocity of the flow in [58] (it seems to be inversely proportional to it). Additional experimental studies show that transport outside cell aggregates is larger than inside them [60]. Outside the boundary layer, advection dominates the transport, while inside the aggregates diffusion is the controlling factor. This motivates the assumption that transport through the cellular aggregate and the boundary layer occurs by diffusion with the same effective diffusion coefficient for the boundary layer and the biofilm [27, 60].

Choosing the oxygen C_o and nutrient C_s concentration at the bulk/boundary layer interface and the boundary layer thickness $d_B(Re)$ as control parameters, the concentrations of nutrients and oxygen inside the region containing the biofilm and the boundary layer [27]

are governed by:

$$D_s \Delta c_s = k_2 \frac{c_s}{c_s + K_s} \frac{c_o}{c_o + K_o}, \qquad (1)$$

$$D_o \Delta c_o = \omega k_2 \frac{c_s}{c_s + K_s} \frac{c_o}{c_o + K_o}, \qquad (2)$$

with zero flux conditions at the substratum. The right hand sides represent the nutrient and oxygen uptake kinetics. Here, ω is the stoichiometric coefficient of the oxygen reaction, k_2 the uptake rate of the nutrient, D_o the diffusion coefficient for oxygen, D_s the diffusion coefficient for the substrate, K_o the Monod half-saturation coefficient of oxygen, and K_s the Monod half-saturation coefficient of the carbon source. The values of all these parameters depend on the bacteria species forming the biofilm. The use of Monod laws makes sense provided the values of the concentrations remain small. Otherwise, inhibition terms should be incorporated. We assume that oxygen is in excess, which is often the case. The concentration of nutrients c_s becomes the limiting concentration c_l, that is, the one that penetrates a shorter distance into the biofilm and therefore constrains division and survival of cells and biofilm growth thereof. The system is reduced to:

$$D_s \Delta c_s = k_2 \frac{c_s}{c_s + K_s}. \qquad (3)$$

For submerged biofilms nutrients and oxygen are both provided by the surrounding flow. Biofilms grown on air/solid surfaces [50] might take oxygen from the air and the substratum, and nutrients from the substratum. In those cases, oxygen and nutrients might become limiting factors in different regions.

At each time step, (3) is solved to reflect changes of nutrient uptake caused by the new biofilm geometry. In our tests, we have computed numerically the solution of the nonlinear boundary value problem for the concentration by using an iterative relaxation scheme with local error control. Solutions for the elliptic problem are constructed as stationary solutions of the diffusion problem. In the tests presented here, error tolerance is set to 10^{-3}. A simple analytical formula creating a concentration distribution inside the biofilm, adapted to its boundary and with a reasonable qualitative dependence on the parameters, was proposed in [27]. That formula may produce useful qualitative predictions at a much lower computational cost if plugged into our stochastic description.
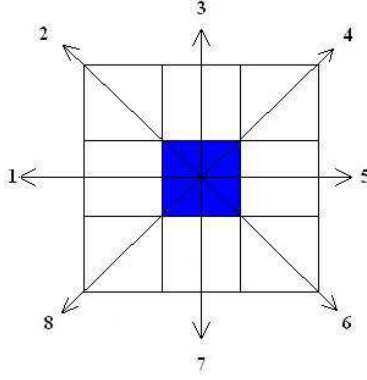
FIG. 7. Neighbor location in the cellular automata description.

B. Erosion by the flow

Surface cells are subject to shear forces exerted by the flow, which may detach them from the biofilm [39, 40]. In principle, cells sheltered by other cells are somehow protected from erosion. Exposed cells will detach with a probability depending on the number and location of their neighbors relative to the motion of the fluid, the biofilm cohesion, which is controlled by EPS matrix generation, and the force due to the flow felt by them, which depends on the Reynolds number. The Reynolds number Re is computed using the hydraulic diameter of the ducts and the average velocity, which are known.

The total force acting on a cell is a balance between the force exerted by the flow and additional forces exerted by its neighbors, depending on their distribution and on the biofilm cohesion. According to the geometry depicted in Figure 5, the force due to the flow is mostly oriented in the x direction. Figure 7 illustrates the location of possible neighbors. Each of them adds a force with a component opposite to the direction of the flow. The strength of each force depends on the position of each neighbor. Let us number the eight neighboring tiles clockwise, starting with the western direction, so that $n_1, n_2, n_3, n_4, n_5, n_6, n_7, n_8$ denote the neighbors located to the west, northwest, north, northeast, east, southeast, south, and southwest, respectively. If the cell has a western neighbor n_1, it is partially shielded from the flow and is unlikely to be carried away. The strongest resistance against the flow is exerted by the eastern neighbor n_5. Next in magnitude are the resistance forces due to adjacent cells n_4 and n_6 located in the northeast and southeast directions, and then n_3 and n_7 in the north and south directions. Neighbors n_2 and n_8 in the northwest and southwest directions

15

add little resistance.

The magnitude of the local force acting on a cell $\mathcal{C}$ can be described by:

$$\tau(\mathcal{C}) = \tau(Re)(1 - \beta(Re)\chi_1(\mathcal{C}))\left(1 - \sum_{i=2}^{8} e_i\chi_i(\mathcal{C})\right). \tag{4}$$

Here, $\tau(Re)$ represents the shear force due to the flow. Solving Navier-Stokes equations outside the biofilm at each step to evaluate it is too costly, especially in turbulent regimes. We are studying small biofilms growing at the wall. Therefore, we approximate it by the shear force at the bottom of an unperturbed rectangular tube. The shear stress at the substratum surface is evaluated from the velocity profiles as $\tau = -\mu\frac{du}{dz}$, where μ is the fluid viscosity. For laminar flows, $\tau(Re)$ is known explicitly: u is given by the Hagen-Poiseuille expression. In general, it can be estimated as

$$\tau(Re) = \frac{f\rho u^2}{2},$$

where u is the known average flow velocity, ρ the fluid density and f the friction factor given by $\frac{16}{Re}$ for laminar flows and $\frac{0.0791}{Re^{0.25}}$ for turbulent flows (see [61, 62]). Notice that the roughness Reynolds number $Re_r = \frac{\rho u e f^{0.5}}{\mu 8^{0.5}}$ is expected to be small, e being the height of the roughness elements.

$\tau(Re)$ is multiplied by a factor that takes into account the geometry of the biofilm and the local support provided by neigbouring cells depending on their distribution. The functions $\chi_i(\mathcal{C})$ in (4) take the value 1 whenever the cell $\mathcal{C}$ has a neighbor located at the position n_i, and vanish otherwise. The factors and weights have been chosen to account for the fact that the fluid flows in the x direction. The weights satisfy $e_i \in (0,1)$, $\sum_{i=2}^{8} e_i = 1$, and $\beta(Re) \in (0,1)$, so that the sign of $\tau(Re)$ is not reversed. In our computer experiments, we have set $e_5 = \frac{5}{17}$, $e_4 = e_6 = \frac{3}{17}$, $e_3 = e_7 = \frac{2}{17}$, $e_2 = e_8 = \frac{1}{17}$. They represent the added resistance against the flow due to neighboring cells depending on their position. $\beta(Re)$ takes values close to 1. If we set $\beta(Re) = 1$, $\tau(\mathcal{C}) = 0$ whenever the cell has a western neighbor. As it departs from 1, the probability of a cell being eroded in presence of the western neighbor n_1 grows. This may be more likely as Re increases.

A probability for cell erosion can be defined following [27]:

$$P_e(\mathcal{C}) = \frac{1}{1 + \frac{\sigma(\mathcal{C})}{\tau(\mathcal{C})}} = \frac{\tau(\mathcal{C})}{\tau(\mathcal{C}) + \sigma(\mathcal{C})}. \tag{5}$$

16

Whenever $\tau(\mathcal{C}) = 0$, we set $P_e(\mathcal{C}) = 0$. Here, $\tau(\mathcal{C})$ is given by (4), and $\sigma(\mathcal{C})$ represents the biofilm strength. A cohesion parameter $\sigma(\mathcal{C})$ varying in accordance with the local EPS generation production is introduced in Section III C. At each time step and for each cell, we generate a random number $r \in (0, 1)$. When $r < P_e(\mathcal{C})$, the cell detaches from the biofilm. Erosion due to the flow may occur as detachment of single cells or of whole clusters of bacteria with a thinning connection to the rest of the biofilm. In Figures 15-20, $\sigma(\mathcal{C})$ is set equal to a constant, to investigate the influence on the biofilm structure of the erosion mechanism we propose. In Figure 24, $\sigma(\mathcal{C})$ varies as described in the next section.

While programming the erosion mechanism, we chose to let two cells be connected if they are neighbors in the grid via any of the 8 neigbouring directions. This is done for several reasons. First, for consistency with division, because the cells divide in each of the 8 directions. Further, if we would only let the 4 main directions connect cells, then newly formed cells with only diagonal connections would break off immediately. We have coded both versions, and simulations show that qualitatively the behavior of the system is unchanged. The difference is that with connections in only 4 main directions the erosion is a little stronger for reasons mentioned above.

C. EPS matrix generation

In small colonies, most bacteria reproduce again and again. As the size of the biofilm grows, the density of cells increases and nutrients and oxygen become scarce. Bacteria start to produce EPS matrix with a certain probability [1]. EPS generation is believed to push newborn cells upwards, inducing vertical growth and making easier access to food and oxygen for them [1], see Figure 2. The EPS matrix also spreads over the neighbouring bacteria making their reproduction harder. As bacteria are deeper in the biofilm, their chances to produce EPS seem to increase because of low concentrations.

The nature of the surrounding flow also influences EPS generation. The stronger the shear due to the flow is, the more resistant the EPS matrix is [39, 43]. Biofilms grown at fixed Reynolds numbers tend to be carried away with the flow as the Reynolds number is increased.

According to these observations, we assume that the probability of a cell producing EPS matrix depends on the availability of nutrients and oxygen at the cell position and the shear

17

exerted by the flow. The EPS matrix is generated with the following probability law:

$$P_{eps}(\mathcal{C}) = R(Re) \left(1 - \frac{c_l(\mathcal{C})}{c_l(\mathcal{C}) + K_l} \right), \tag{6}$$

where $R(Re) \in (0,1)$ and c_l represents the limiting concentration. Cell decay may be taken care of by deactivating cells at which the concentration falls below a critical value. Concentrations at each cell $\mathcal{C}$ are stored in a linked list of cells. These lists are updated once a time step has been completed, to reflect the change in the biofilm geometry. The concentrations are computed as described in Section III A.

As expected [1], the probability (6) takes small values when the biofilm thickness does not surpass a threshold (the limiting concentration is large enough) and increases as the cell is deeper into the biofilm (the limiting concentration will decrease).

At each time step and for each cell, we generate a random number $s \in (0,1)$. When $s < P_{eps}(\mathcal{C})$, the cell will generate EPS. After several steps, the fraction of cells generating EPS matrix stabilizes to a certain value, that may be used to determine $R(Re)$ by comparison with experimental measurements. Whereas $R(Re)$ controls the percentage of cell generating EPS matrix, the factor involving the concentration governs the spatial distribution of these cells in the biofilm.

The amount and nature of the EPS matrix produced determines the cohesion (strength) of the biofilm. Parameters representing the biofilm cohesion can be measured [43, 55] and introduced in the erosion probability law (5). However, it may be useful to have a rough idea of its spatial variations and their effect, to infer how the presence of weaker regions may affect biofilm evolution or to input this information in macroscopic models.

The EPS matrix diffuses and accumulates in different ways in different biofilms [33, 34]. We test here a local measure σ of the biofilm cohesion which takes into account the number of neighbors and their nature:

$$\sigma(\mathcal{C}) = \frac{\sigma_0(Re)}{8} \sum_{i=1}^{8} \sigma_i(\mathcal{C}), \tag{7}$$

where

$$\sigma_i(\mathcal{C}) = \begin{cases} 0 & \text{if neighbor } n_i \text{ is not present} \\ \alpha & \text{if neighbor } n_i \text{ is present, but does} \\ & \quad \text{not produce EPS matrix} \\ 1 & \text{if neighbor } n_i \text{ produces EPS matrix} \end{cases} \tag{8}$$

18

and $n_1(\mathcal{C})$, $n_2(\mathcal{C})$,...,$n_8(\mathcal{C})$ denote the eight neighbor locations for the cell under study (see Figure 7) and $\sigma_0, \alpha > 0$. When deactivated cells are present an additional constant α' should be used for them. Other options are possible. $\sigma(\mathcal{C})$ might be modulated by the variations of the concentration of EPS matrix, governed by equations similar to those described in Section III A when the matrix diffuses easily.

The parameters σ_0, α represent the strength of the EPS matrix generated by the bacteria and the strength of the attachment between standard bacteria. In practice, σ_0 seems to increase with Re [38, 39, 43]. They depend on the type of bacteria and must be fitted experimentally. We have selected $\alpha = \frac{1}{2}$ in our computer experiments. Figure 24 includes the variable cohesion in the erosion mechanism.

For specific bacteria forming biofilms on air/agar interfaces in absence of flow, there are detailed measurements of the fractions of cells generating EPS and related chemicals. Precise visualizations of their spatial distribution within the biofilm are available too [50]. Regions with large availability of nutrients contain normal cells. As the concentration of nutrients decreases, the percentage of cells generating EPS matrix increases, and they may even deactivate. In that specific case, EPS matrix production is known to be triggered by cell production of several chemicals. We are not aware of such detailed studies for biofilms in flows yet, but the laws described here might be updated to incorporate such knowledge if it ever becomes available.

D. Cell division

The mechanism for cell reproduction is similar to that in [27], except for the fact that EPS producers and deactivated cells do not undergo cellular division in the same step. At each time step, and once we have checked which cells produce EPS matrix, the remaining cells $\mathcal{C}$ will divide with probability:

$$P_d(\mathcal{C}) = \frac{c_l(\mathcal{C})}{c_l(\mathcal{C}) + K_l}, \tag{9}$$

where c_l denotes the limiting concentration and K_l its saturation coefficient in the Monod law. The concentration is computed at the beginning of each step as described in Section III A. We are neglecting changes in concentration due to newborn cell consumption or cell switching to EPS generation within the same step.

At each time step, and for each cell not generating EPS matrix, we compute a random number $p \in (0, 1)$. If $p < P_d(\mathcal{C})$, the cell will divide. Whenever neighboring grid tiles are empty, the daughter cell is placed in any of the empty tiles with equal probability. Otherwise, the new cell will shift one of the neighbors. The cell offering the minimal mechanical resistance is chosen, that is, the one lying in the direction of shortest distance from the reproducing cell to the biofilm boundary/bulk layer. The same rule should be applied to the shifted cell: it either occupies adjacent empty tiles with equal probability or shifts a neighboring cell in the direction of smallest mechanical resistance. However, to reduce the computational cost we shift neighboring cells in the same direction. This process is repeated until all the displaced cells have been accommodated.

E. Adhesion of floating cells

The adhesion mechanism assumes that we know the number of bacterial cells that are floating in the flow and the adhesion rate. Let $N_f(t)$ be the number of cells carried by the flow at time step t. The number of cells that will attach to the bottom surface at time t will be a fraction of the number of floating cells, larger or smaller depending on the Reynolds number, the type of surface and the bacteria species. Raising the Reynolds number we increase the probability of hitting the surface. Whether the bacteria successfully attach will rely on the interaction between the specific type of bacteria and surface we are working with. Thus, the number of attached cells will be:

$$N(t) = [\gamma N_f(t)], \tag{10}$$

where $[\,]$ denotes the integer part and γ is a parameter which measures the likeliness of that specific bacteria to attach to that surface. It can be seen as an adhesion rate. Bacterial likeliness to attach to a surface depends on the type of flow and the nature of the substratum [29]. In laminar flows the main mechanism driving particles to the wall seems to be Brownian motion [63]. This usually results in low deposition rates for laminar flows. As the Reynolds number increases, turbulent effects play a role and particle deposition rate increases linearly with the Reynolds number for small Stokes numbers [63]. It has been experimentally observed that the residence time of bacteria hitting a wall increases with shear [30] and that biofilm accumulation tends to be larger for larger flows [42]. Thus, $\gamma(Re)$ is likely to increase with Re.

To decide where these cells are going to be attached, we assign a number to any surface compartment (of either substrate or biofilm, both are considered together), producing a list of S numbers. Then, we generate N random integers between 1 and S. We locate new cells at those positions. This assumes equal probability for all the surfaces as adhesion sites. Numerical tests implementing this mechanism are shown in Figures 21 and 23. Whenever precise information on preferential adhesion sites is available, as in [55], the adhesion strategy should be changed to account for that fact.

F.   Nondimensionalization and parameters

Nondimensionalizing the model is essential to identify the minimum number of independent parameters, or to be able to distinguish what is large and what is small. All the probabilities we have introduced are dimensionless. Dimensions enter the model mainly through the concentration, length and time scales:

- Length: The basic distance considered in the model is the size of a bacteria a, about 2 or 1 micrometers. It is set equal to 1 in our tests.

- Time: In the model, time is not given explicitly. It appears in the number of time steps carried out at each simulation. A simple estimate for the time step size can be given: in the most favorable conditions for bacterial reproduction, the concentration is so high that the probability of reproduction is approximately one. In these conditions, the bacterial population will double in a single time step. An upper bound for the time step, which allows to relate computational T and experimental times is the minimum doubling time:
$$t = \frac{\ln(2)}{\nu_{max}},$$
where ν_{max} is the growth rate, which is a known parameter for some bacterial species and nutrients.

- Concentration: The concentration field is calculated solving a boundary value problem for the limiting concentration, which involves a number of constants with their units that must be nondimensionalized. Making the changes of variables:
$$\hat{c}_l = \frac{c_l}{K_l}, \ \hat{C}_l = \frac{C_l}{K_l}, \ F_l = \frac{k_l a^2}{2 D_l K_l}, \ \delta_B = \frac{d_B}{a}, \hat{x} = \frac{x}{a},$$

21

we get the dimensionless equations:

$$\hat{\Delta}\hat{c}_l = 2F_l\frac{\hat{c}_l}{\hat{c}_l + 1}.$$ (11)

with boundary condition $\hat{C}_l$ at the bulk/boundary layer interface.

The four parameters a, k_l, D_l, K_l are reduced to one: F_l, which is analogous to the Thiele modulus and measures the ratio of the uptake rate to the diffusional supply. Typical values for bacteria commonly used in flows, like Pseudomonas Aureaginosa or Pseudomonas Putida, and standard nutrients produce values in the range $10^{-8} - 10^{-2}$. Notice that in all the formulas introduced in previous sections, only quotients $\frac{c_l}{c_l + K_l} = \frac{\hat{c}_l}{\hat{c}_l + 1}$ are involved. All combinations of parameters producing the same value F_l for fixed values of the remaining parameters produce the same results.

The tables below summarize the different parameters used through the text. For fixed bacterial strains, nutrients, surfaces and flows, the parameters a, ε, λ, δ, C_s, C_o, D_s, D_o, ω, Re, ρ, μ, $N_f(t)$ are usually known. The parameters describing the bacterial kinetics for the particular choice of nutrient k_2, K_s, K_o, ν_{max} are only available in some cases. In general, they have to be measured. The same happens with the average cohesion $\sigma_0(Re)$ or the adhesion rate $\gamma(Re)$. The boundary layer thickness $d_B(Re)$ may be estimated experimentally for a given flow regime. σ_0 and α in (7) might be calibrated using experimental measurements on the percentage of biofilm cells generating EPS matrix and its cohesion. The specific values of $e_2, ..., e_8$ in (7) are not too relevant. Replacing them by other positive values respecting the symmetry produces similar results. The dependence on temperature in the model is implicit through the uptake rates, the density and viscosity of the fluid, and the diffusivities.

IV. THREE DIMENSIONAL MODEL

The model can be extended to three dimensions with simple changes. Biofilms grow on the bottom of a rectangular pipe carrying a flow containing nutrients, as shown in Figure 8. Space is partitioned in a grid a cubic tiles, of size a. Again, each of them is filled with one bacterium, fluid or substratum. Bacteria reproduce, spread, detach, decay and generate EPS matrix according to the rules described in Section III, with the changes we describe below.
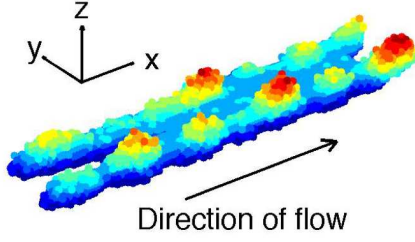
FIG. 8. Three dimensional biofilm growing on the bottom of the pipe.
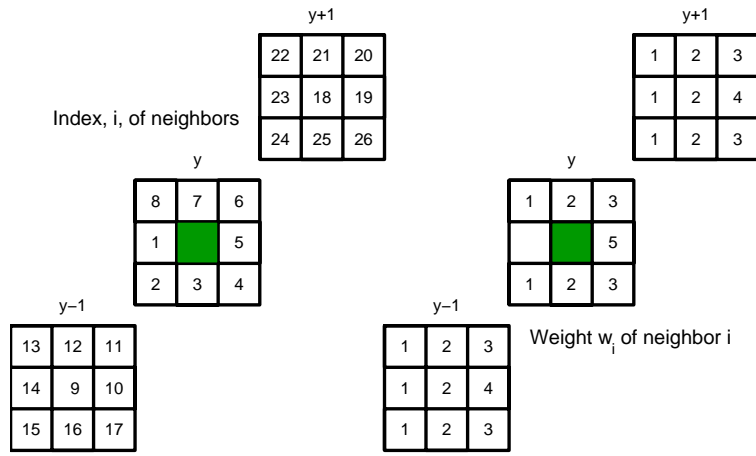

FIG. 9. Neighbors and weights for three dimensional biofilms.

The probabilities for EPS generation and cell division are still given by (6) and (9), respectively. Quotients $\frac{c_l}{c_l + K_l} = \frac{\hat{c}_l}{\hat{c}_l + 1}$ are involved, where the dimensionless limiting concentration field is computed by solving numerically the three dimensional version of the nonlinear boundary value problem for the concentration. We use a relaxation method to compute numerically the solutions.

The erosion probability has the form (5), where $\tau(\mathcal{C})$ is given by (4) with $\sum_{i=2}^{8} e_i \chi_i(\mathcal{C})$ replaced by $f(\mathcal{C})$:

$$f(\mathcal{C}) = \frac{1}{2} f_y(\mathcal{C}) + \frac{1}{4}(f_{y+1}(\mathcal{C}) + f_{y-1}(\mathcal{C})), \qquad (12)$$

$$f_{y-1} = \frac{1}{19} \sum_{i=9}^{17} w_i \chi_i(\mathcal{C}), \quad f_{y+1} = \frac{1}{19} \sum_{i=18}^{26} w_i \chi_i(\mathcal{C}), \quad f_y = \frac{1}{17} \sum_{i=2}^{8} w_i \chi_i(\mathcal{C}).$$

$\tau(Re)$ represents the shear at the bottom wall. This assumes that the patterns remain

23

near the wall. Explicit formulas for laminar flows are available in ducts with rectangular section [64], and approximations for turbulent flows can be found in cite [65]. Numerical simulations in Figures 10-14 set $\tau(Re)$ equal to a constant to simplify. The functions $\chi_i(\mathcal{C})$ take the value one whenever the cell has a neighbor located at the position n_i, respectively, and vanish otherwise. n_i, $i = 1, .., 26$, denote the neighbors of the cell under study n_0, see Figure 9. The weights w_i are chosen to account for the fact that the fluid flows mostly in the x direction. In our simulations, the weights w_i are slightly larger for neighbors located in the intermediate slice of the cube, which contains the cell whose neighbors we are tracking. The weights are equal for neighbors occupying the same position in each of the two lateral slices. Figure 9 illustrates the numbering of neighbors and the weights we have used in our simulations. The local cohesion in (5) may be constant or take the form:

$$\sigma(\mathcal{C}) = \frac{1}{3}(\sigma_y(\mathcal{C}) + \sigma_{y-1}(\mathcal{C}) + \sigma_{y+1}(\mathcal{C})), \tag{13}$$

where $\sigma_y(\mathcal{C})$ is given by (7) applied to the slice containing the cell. $\sigma_{y+1}(\mathcal{C})$, and $\sigma_{y-1}(\mathcal{C})$ are given by a similar formula, but replacing 8 by 9 and summing up over all the neighbors in the lateral slices.

V. NUMERICAL RESULTS

In this section, we illustrate the evolution of several initial configurations under different conditions, to gain understanding of the influence of the controlling parameters and the interaction between competing mechanisms.   First, we analyze the evolution of a biofilm seed for constant biofilm cohesion σ, considering only the growth and erosion mechanisms for different shear and nutrients on either flat or rough surfaces. Then, we implement the adhesion mechanism on uncolonized surfaces. Finally, we include the EPS generation mechanism. Fixing the initial conditions, a well defined qualitative behavior is observed in all the simulations. We usually set F_l (that is, the nutrient and the type of bacteria) and vary the flow or the concentration. The parameter values we use do not correspond to any specific bacteria-nutrient choice, since adequate experimental data for parameter calibration are not available yet.

The first numerical experiments show three dimensional patterns with $\sigma(\mathcal{C}) = \sigma$, and $\tau(Re)$ also a constant. The ratio $\frac{\tau(Re)}{\sigma}$ is a control parameter. The initial seed is the same

in all the tests: a slab containing $110 \times 20 \times 4$ cells. Two erosion processes are observed: sloughing of large fragments, and smooth erosion of surfaces. When the shear is large enough compared to the biofilm cohesion ($\frac{\tau}{\sigma}$ large) and the limiting concentration is not too high, the initial layer of biofilm remains almost flat and homogeneous while it is slowly washed out, see Figure 10. Cells are eroded from the front, but may grow downstream. Biofilms that are not strong enough have been experimentally observed to be washed out on glass surfaces in [43]. This happens typically to biofilms created at lower Reynolds number when the shear is increased.

Decreasing the ratio $\frac{\tau}{\sigma}$ or increasing slightly the concentration, the initial biofilm seeds develop ripple-like patterns, that advance downstream with the flow, as in Figure 11. Ripples anchor and become streamer-like structures (fingers or peaks elongated in the direction of the flow) for smaller $\frac{\tau}{\sigma}$ or larger concentrations, see Figures 12 and 13(a). Fingers that become too large may detach. Ripples traveling downstream on top of lower layers of biofilm have been reported for both laminar and turbulent flows in [39, 41]. Networks of streamers being eroded and leaving small ripples behind have been experimentally observed in [39]. Low enough ratios $\frac{\tau}{\sigma}$ or large enough concentrations lead to networks of mounds or towers separated by voids, as in Figure 13(b) and Figure 14, where F_l is increased so that towers are more clearly noticed with fewer cells. Similar patterns are commonly observed in nature in low shear environments, see [49].

The evolution of the cellular aggregates reproduced in these 3D simulations includes only growth and erosion processes. What are the precise mechanisms producing different ripples or streamers observed in real biofilms (in both laminar and turbulent regimes) is uncertain, though mechanical effects are believed to be relevant. Cell displacement due to the flow, decay and cell adhesion should also be considered to gain insight on the processes that trigger real pattern formation.

The observed patterns depend on the combination of parameters selected: F_l, δ_B, $\hat{C}_l$ and $\frac{\tau}{\sigma}$. When only growth processes are taken into account, vertical fingers are formed if the growth dynamics is constrained by the limiting concentration, see [24, 66]. If a large enough concentration reaches most cells, biofilms tend to be flatter. According to the equations that govern the concentration, different factors may favor this:

- Decreasing F_l reduces nutrient/oxygen uptake by the cells and increases the average values of the limiting concentration field for a fixed biofilm geometry, δ_B and $\hat{C}_l$. F_l
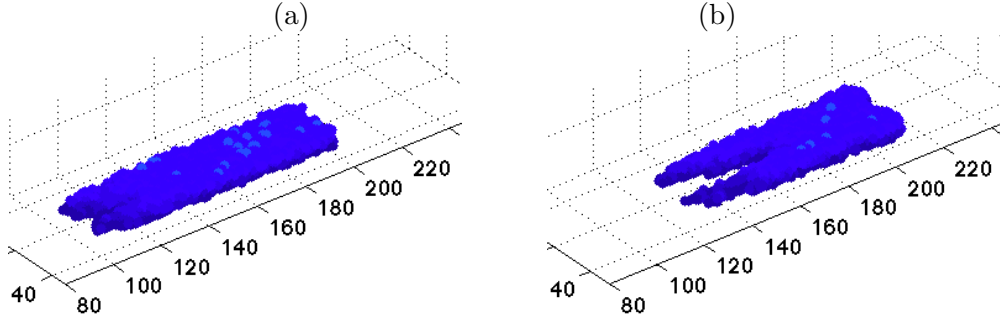
25

FIG. 10. An initially flat and homogeneous biofilm being washed out by the current. Snapshots are taken at steps $T = 20$ and $T = 60$. After 200 steps all cells have eroded. Dimensionless parameter values: $\hat{C}_l = 2.25$, $F_l = 0.04$, $\delta_B = 5$, $\frac{\tau(Re)}{\sigma} = 5$, $\beta = 1$.
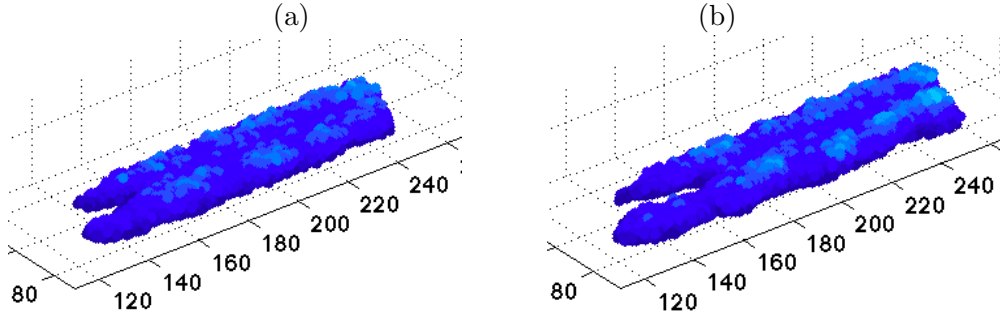

FIG. 11. A flat and homogeneous biofilm seed develops ripple-like patterns moving downstream with the flow. Snapshots are taken at steps $T = 50$ and $T = 80$. A peak located at grid position 200 clearly migrates to position 220. Same parameter values as in Fig. 10 except $\frac{\tau(Re)}{\sigma} = 2$.

depends on the nutrient type and the bacterial species through uptake rates, saturation and diffusion coefficients. Therefore, it is fixed for specific choices of bacteria and nutrient. The threshold concentration to hinder fingering can only be reached if the limiting concentration in the fluid $\hat{C}_l$ is large enough depending on F_l and the biofilm thickness.

- Decreasing the boundary layer thickness δ_B also increases the concentration field, for a fixed biofilm geometry, F_l and $\hat{C}_l$. However, concentrations that are large enough uniformly can only be reached if the limiting concentration in the fluid $\hat{C}_l$ is large enough. In practice, δ_B decreases with the flow velocity. Rising the flow velocity might increase everywhere the concentration field and favor flatter biofilms.
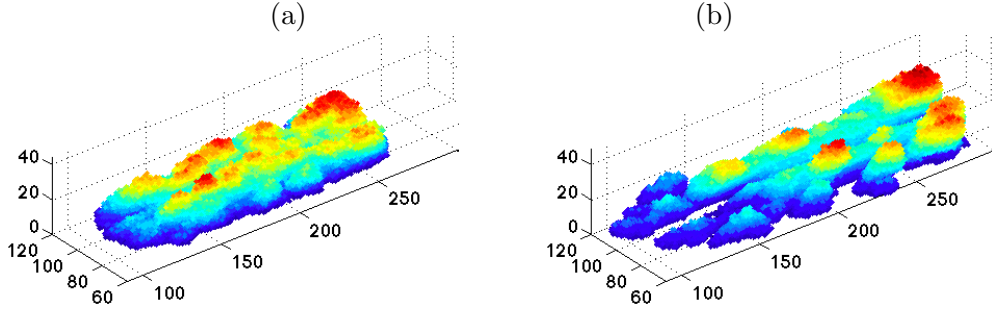
FIG. 12. A flat and homogeneous biofilm seed generates streamer-like structures. Same parameter values as in Fig. 11 except $\frac{\tau(Re)}{\sigma} = 1.5$. Snapshots are taken at steps $T = 80$ and $T = 160$ (75089 alive cells).
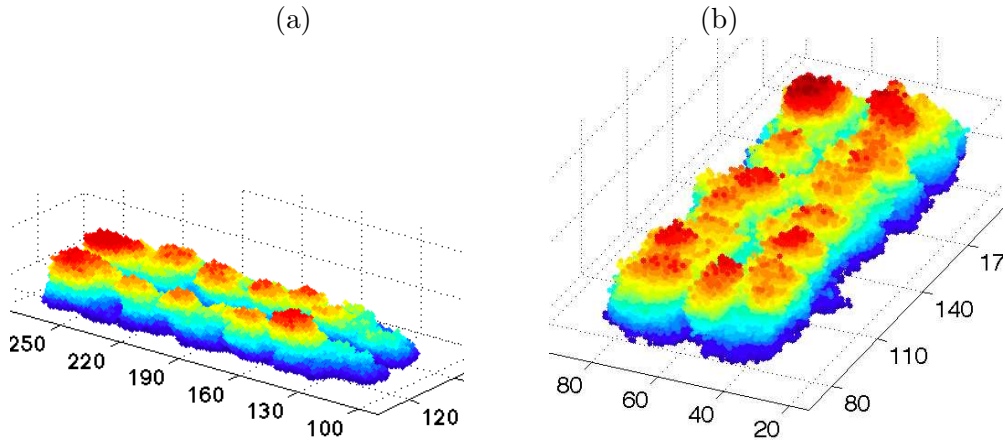

FIG. 13. (a) Increasing the outer concentration in Fig. 11 we also find streamer-like structures. Snapshot taken at $T = 80$ for $\hat{C} = 3$ (71516 alive cells). (b) Further decreasing $\frac{\tau(Re)}{\sigma}$ in Fig. 12 we generate mounds. Snapshot taken at $T = 70$ for $\frac{\tau(Re)}{\sigma} = 0.5$ (88815 alive cells).

- Choosing $\hat{C}_l$ large enough depending on the biofilm geometry, F_l and δ_B, we may end up with flatter biofilms. Their thickness will increase with time, unless we are able to choose a current strong enough to keep them thin. However, that might in turn generate patterns by a different mechanism, or just wash out the biofilm on smooth surfaces.

In intermediate regimes we may see all sorts of dendritic or porous patterns, especially in two dimensions. The above remarks apply in static or very slow flows. As the ratio $\frac{\tau}{\sigma}$ grows, the erosion mechanism modifies the picture. It may modify or suppress patterns or
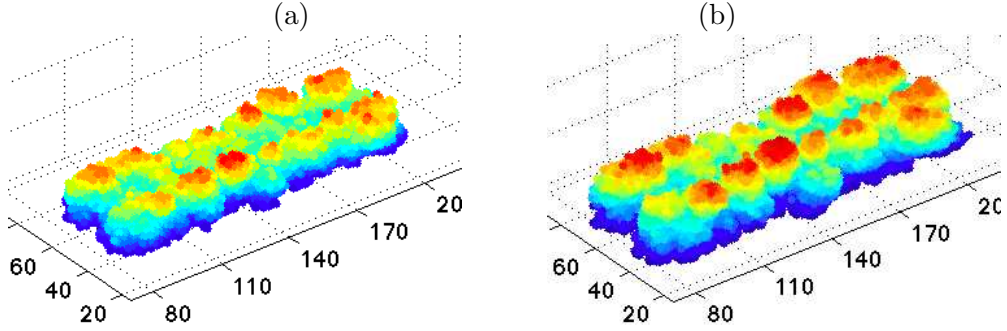
FIG. 14. A biofilm seed forms a group of mounds. Same parameter values as in Fig. 13(b) except $F = 0.08$. Snapshots are taken at steps $T = 70$ and $T = 100$ (63534 alive cells).

create additional ones depending on the values of $\frac{\tau}{\sigma}$ and δ_B. Strong erosion does not require large flows, small biofilm cohesion suffices. Increasing the concentration, we may reduce or overcome erosion effects as in Figures 13(a) or 19(b).

Two dimensional simulations produce similar results to 3D simulations, though the patterns tend to be more branchy. The thresholds separating flat biofilms, wavy biofilms, mounds and streamer-like or mushroom-like patterns are shifted. Depending on F_l and $\hat{C}_l$, some of the regimes observed as we vary $\frac{\tau}{\sigma}$ may almost vanish.

We revisit our three dimensional simulations on smooth and rough surfaces using the two dimensional model. Almost all the simulations start from an initial biofilm seed containing 110×4 cells. Roughness adds another variable that interacts with the growth and erosion mechanisms. We represent it by the peaks depicted in Figure 6. Some roughness patterns may prevent the washing out effect described before as $\frac{\tau}{\sigma}$ increases. In Figure 15 (c)-(d), 2×2 square peaks with an interpeak space of 5 tiles help the biofilm the remain attached to surfaces they have already colonized and expand onto neighboring downstream regions. It is washed out on a smooth surface, see Figure 15 (a)-(b). Reducing the spacing between peaks to 2 tiles, we see a similar behavior with less cells and flatter biofilms, since cells have less space to reproduce. Increasing the spacing to 10 tiles, the evolution is similar. However, biofilms contain more biomass since cells have more space to divide and spread. If this spacing increases further, the sheltering effect of roughness decreases. If the depth of the steps increases, nutrients become too scarce to sustain the cell population, hindering biofilm survival. Considering several biofilm peaks as initial data instead of flat layers, we see a similar evolution. Biofilms are washed out on a flat substratum. Surface roughness of
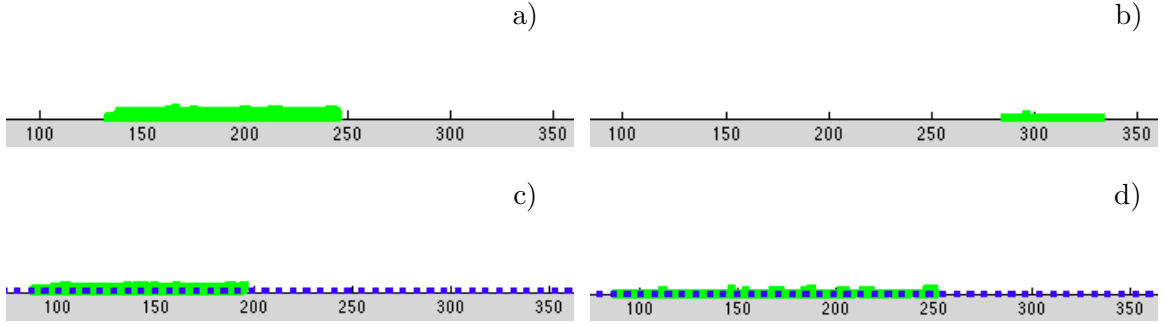
FIG. 15. (a), (b) Snapshots showing a biofilm being washed out over a flat substratum for large enough $\frac{\tau(Re)}{\sigma}$. (c), (d) On a rugose surface, with steps characterized by peak height $\epsilon = 2$, length $\lambda = 2$, and interpeak distance $\delta = 5$, the biofilm front is anchored and the biofilm expands colonizing new regions downstream. Dimensionless parameter values: $\frac{\tau(Re)}{\sigma} = 5$, $F_l = 0.04$, $\hat{C}_l = 1.5$, $\delta_B = 5$, $\beta = 1$. Time between snapshots: 450 time steps.

the same order of magnitude as the bacterial size helps the peaks to colonize neighbouring regions and merge, producing more uniform covers, as in Figure 16. Biofilms succeed in expanding upstream. Other roughnesses may have different effects.

Decreasing the ratio $\frac{\tau(Re)}{\sigma}$, we find a new regime in which ripple-like patterns are observed. Newborn cells accumulate downstream, forming ripples and a floating finger at the rear of the biofilm, which eventually reattaches allowing the biofilm to expand downstream, see Figure 17 (a)-(b). More limited upstream expansion may also occur. Roughness anchors the front of the biofilm, fostering colonization of downstream regions, as in Figure 17 (c)-(d). Thicker biofilms with more noticeable ripples seem to be formed. Further decreasing $\frac{\tau(Re)}{\sigma}$, fingers aligned with the flow develop, which detach when they surpass a certain size. Figures 18 (a)-(b) show the biofilm evolution on a flat substratum. For smaller $\frac{\tau(Re)}{\sigma}$, branchy biofilm towers separated by fluid grow on the initial biofilm, as in Figure 19 (a). When $\hat{C}_l$ is increased, mushrooms are more easily formed, that become denser and merge for higher values of $\hat{C}_l$, as in Figure 19 (b).

All the previous numerical simulations set $\beta = 1$ in (4). That assumes that cells only feel the influence of the flow in the x direction. We have repeated the previous simulations for $\beta \in (0.9, 0.99)$ finding an increasing chance of long biofilm layers splitting in smaller patches, that may eventually be washed out, and a reduction in the maximum height of the patterns. Otherwise, similar trends are observed provided the concentration is large
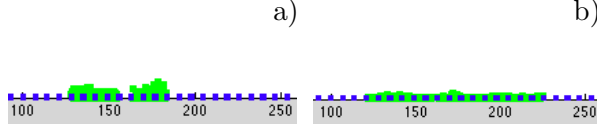
a)   b)

FIG. 16. Same as Figure 15 starting from two small colonies, which merge and expand helped by roughness, downstream but also slightly upstream. On a flat substratum they are washed out.

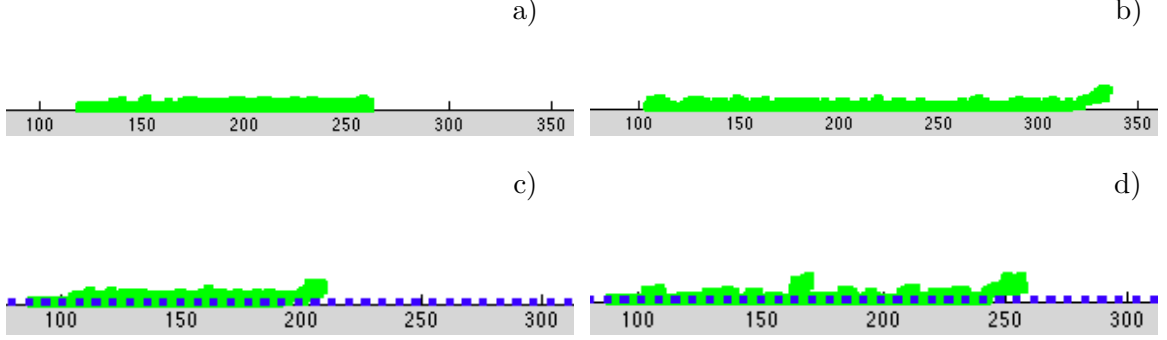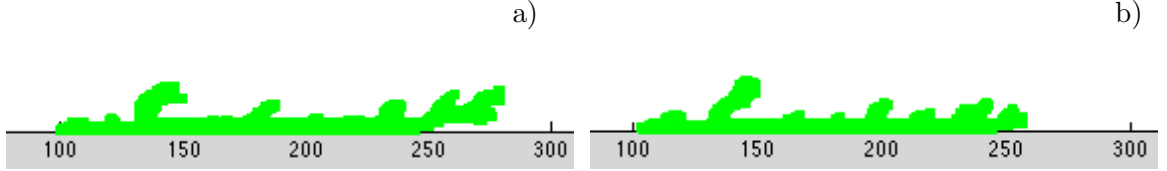a)   b)

c)   d)

FIG. 17. Ripple-like structures form on an initially flat seed: (a), (b) over a flat substratum, (c), (d) on a rugose surface with steps characterized by peak height $\epsilon = 2$, length $\lambda = 2$, and interpeak distance $\delta = 5$. Dimensionless parameter values: $\frac{\tau(Re)}{\sigma} = 2$, $F_l = 0.04$, $\hat{C}_l = 1.5$, $\delta_B = 5$, $\beta = 1$. Time between snapshots: 800 time steps.

a)   b)

FIG. 18. Fingers curved with the flow develop in a biofilm over a flat substratum: a) Time step $T = 300$. (b) Time step $T = 500$. The trailing finger has eroded, it will grow again later. The biggest finger at the front detached but has grown again. An intermediate finger has also detached, leaving room for another one at its back to grow. Dimensionless parameter values: $\frac{\tau(Re)}{\sigma} = 1$, $F_l = 0.04$, $\hat{C}_l = 1.5$, $\delta_B = 5$, $\beta = 1$.

enough to compensate the increased erosion. In Figure 20 (a), an initially flat biofilm seed breaks into separated patches. Increasing the concentration, the biofilm splits in patches that evolve into streamer-like patterns, see Figure 20 (c). Decreasing $\frac{\tau}{\sigma}$, a stable network of biofilm towers separated by fluid channels develops in Figure 20 (d). Figure 20 (b) shows the effect of roughness, compared to subplot (a). In practice, as Re grows turbulent effects may
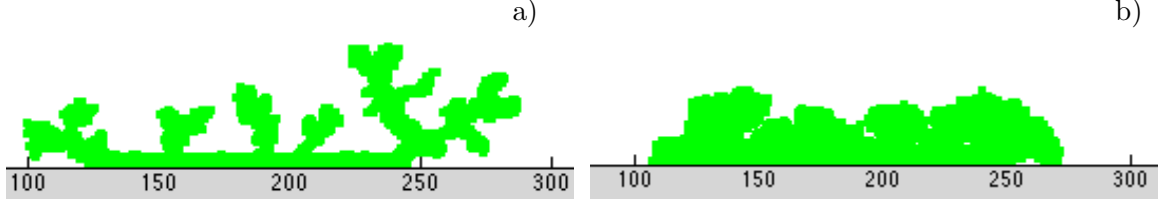
FIG. 19. (a) Same as Figure 18 for smaller $\frac{\tau(Re)}{\sigma} = 0.25$. An expanding network of biofilm branches infiltrated with fluid is formed. (b) Same as Figure 18 increasing the limiting concentration to $\hat{C}_l = 2.7$. The biofilm expands forming dense mushrooms separated by narrow channels, that eventually merge.

be important and the model should allow for a degree of erosion in the z direction. As Re increases, $\beta(Re)$ should probably diminish, enhancing erosion by the flow. However, there are a number of overlapping competing effects with uncertain outcome. The thickness of the concentration boundary layer $\delta_B(Re)$ should also decrease, augmenting the concentration of nutrients, and growth rates thereof. In case floating cells are present, adhesion rates might equally increase with Re, leading to larger biofilm accumulation [42].
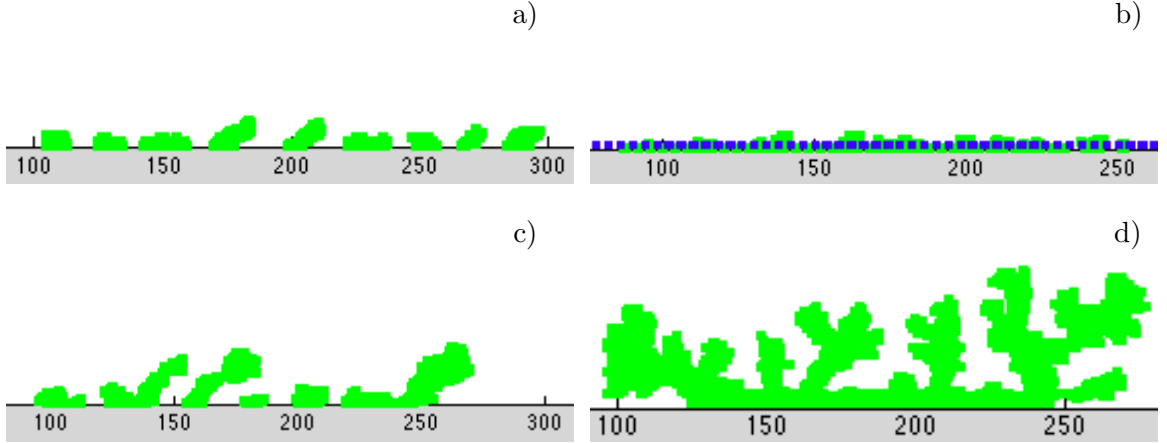

FIG. 20. Evolution of a flat biofilm seed when $\beta \neq 1$. (a) $\frac{\tau}{\sigma} = 2$, $\hat{C}_l = 1.5$, $\beta = 0.99$, $\delta_B = 5$, $F_l = 0.04$, $T = 600$. The biofilm breaks into patches that generate small peaks. (b) Same parameters as (a) except $\frac{\tau(Re)}{\sigma} = 5$, on a rough surface. Fingers are eventually eroded, leaving a thin biofilm behind. (c) Same parameters as (a) with increased $\hat{C}_l = 1.8$. Streamer-like structures are formed, that detach when they become too large. (d) Same parameters as (c) with smaller $\frac{\tau(Re)}{\sigma} = 0.25$. An expanding network of biofilm branches develops.

So far we have only considered the evolution of attached biofilm seeds, neglecting the pos-

sible adhesion of floating cells. Figure 21 shows the evolution of an uncolonized substratum under a flow carrying nutrients and bacteria. The initial state is the same in all the trials, a clean surface. The density of bacteria, oxygen and nutrients carried by the flow is also the same in all the figures. The ratio $\frac{\tau}{\sigma}$ and the number of attached cells N vary. For high enough adhesion rates the biofilm may cover completely the bottom of the pipe provided the rate of adhesion of bacteria is high enough compared to the erosion effects, see Figure 21(a). Biofilm patches form, which eventually merge. After some time, the substratum is fully covered by wavy biofilm layers of increasing thickness. Otherwise, only patches, or isolated peaks grow, see Figure 21(b). It has been experimentally observed in [44] that low adhesion rates at low Reynolds numbers lead to patchy configurations, see Figure 1. Larger adhesion rates at larger Reynolds numbers have produced rippled biofilm layers, see Figure 4.
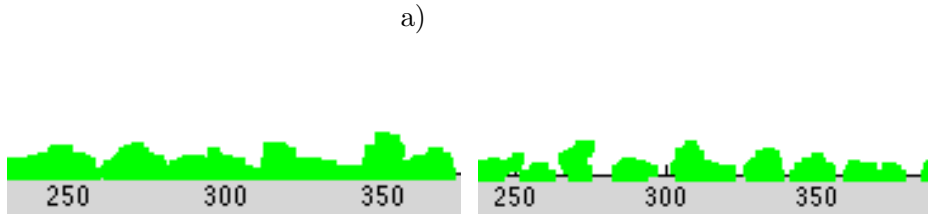
a)   b)

FIG. 21. (a) Biofilm growth at large adhesion rates. A wavy biofilm carpet is formed when $\frac{\tau(Re)}{\sigma} = 2.5$ and $N = 80$. (b) Biofilm grown at smaller adhesion rates. Scattered patches are generated when $\frac{\tau(Re)}{\sigma} = 1$ and $N = 10$. Other dimensionless parameter values are $\hat{C}_l = 1.5$, $\beta = 0.99$, $F_l = 0.04$ and $\delta_B = 5$. Snapshots are taken at time step 75.

The length scales in the patterns when erosion effects are low seem to be governed by the average concentration the cells feel. Low concentrations seem to increase the distance between patterns. Raising F_l and δ_B produces that effect. Figures 22(a)-(b) show the effect of δ_B. For small δ_B, flat dense biofilms may be formed, see Figure 22(a). Small F_l would have a similar effect. Increasing F_l or decreasing $\hat{C}_l$, protuberances appear again. For larger δ_B, fingers are formed at increasing distances, see Figures 18, 19, 22(b), or Figure 23(a), which includes also adhesion. Figures 13 (b) and 14 illustrate variations in the patterns with F_l. Taking only into account erosion and growth, the boundary layer thickness δ_B was shown in [27] to control the distance between patterns for fixed F_l. Notice that in [27], $\tau(\mathcal{C})$ in (4) is set equal to a constant and the resulting fingers do not see the direction of the
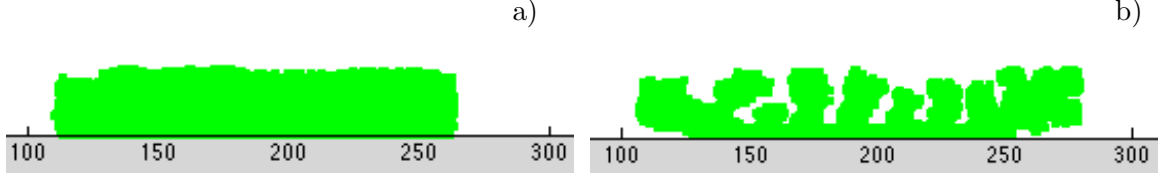
32

FIG. 22. (a) Biofilm for a small boundary layer thickness $\delta_B = 1$. A flat biofilm seed evolves into a thickening dense biofilm. (b) Biofilm evolution for an increased boundary layer thickness $\delta_B = 3$. A mushroom network develops. Other dimensionless parameter values are $\frac{\tau(Re)}{\sigma_0} = 2$, $\hat{C}_l = 1.5$, $\beta = 1$, and $F_l = 0.04$. Snapshots are taken at time steps 25 and 75, respectively.

flow. In static flows, the distance between fingers is shown to increase as the availability of nutrients diminishes in [24]. Additionally, the erosion mechanism can generate, suppress or modify patterns. It can erode and curve the fingers that would grow in absence of flow or change initial distances between fingers. Some of them may detach when they surpass a certain size, leaving just a few, or only one at the end, or they may detach and grow in turn. Adhesion mechanisms further modify the picture, see Figure 23 (b), where peaks have been replaced by wavy layers.
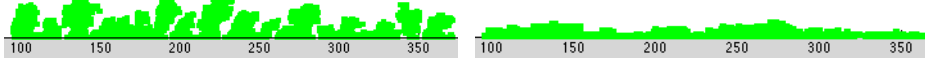

FIG. 23. Variations of the boundary layer thickness including adhesion. (a) Biofilm evolution after 50 time steps when $\delta_B = 3$. A network of biofilm towers separated by fluid is grown. (b) Biofilm evolution after 50 time steps when $\delta_B = 7$. The surface is covered by a wavy carpet of biofilm. Other parameter values are are $\hat{C}_l = 1.5$, $\beta = 0.99$, $\frac{\tau}{\sigma} = 2$, $N = 60$, $F_l = 0.04$.

In the previous figures, the cohesion parameter σ was set equal to a constant. The remaining figures incorporate the EPS generation mechanism for σ given by (7) in absence of floating cells. Compare Figures 17 and 18 to Figures 24(a)-(b). Resulting biofilms are more rigid. As $\frac{\tau(Re)}{\sigma_0(Re)}$ is further reduced, biofilm towers are stronger and do not deviate in the direction of the flow, see Figure 24(c). In these figures, σ varies locally, depending on the number of bacteria generating EPS matrix, and the values we give to the parameters σ_0 and α, representing the strength of the EPS matrix and standard attached cells of a specific bacteria species. The percentage of cells producing EPS matrix remains stable during the
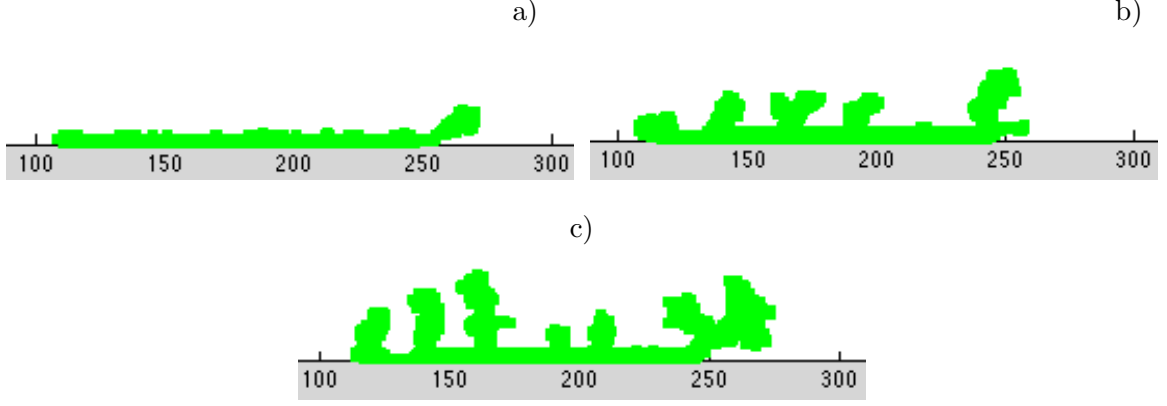
FIG. 24. Tests including the EPS generation mechanism. The constant cohesion parameter σ is replaced by a self-adjusted variable cohesion parameter σ given by (7): (a) Small ripples are formed when $\frac{\tau(Re)}{\sigma_0(Re)} = 2$, $R(Re) = 0.4$. (b) Peaks curved in the direction of the flow develop on more compact biofilms when $\frac{\tau(Re)}{\sigma_0(Re)} = 0.5$. (c) Vertical towers appear when $\frac{\tau(Re)}{\sigma_0(Re)} = 0.25$. The symmetry of the pattern shows a decreasing dependence on the flow direction. Other dimensionless parameter values: $\hat{C}_l = 1.5$, $\delta_B = 5$, $\beta = 1$, $F_l = 0.04$, $T = 150$.

biofilm evolution and might be used to calibrate σ_0 and α, since this is a parameter that can be measured experimentally in real biofilms. Matrix generation affects growth and local consistency. The thresholds separating different pattern regimes are apparently shifted.

In general, the role of the controlling parameters once the type of bacteria and nutrient is fixed seems to be the following. In absence of floating cells, the parameter F_l appears to regulate the critical thickness for the biofilm to survive and the regimes for patterns. Small F_l due to small uptake rates may result in mostly flat patterns. Large F_l due to small diffusivities may result in mostly tower-like structures. Once F_l is fixed, δ_B has a similar effect and the ratio between the shear due to the flow and the biofilm cohesion determines the degree of erosion of the biofilm by the flow. It competes with the concentration to determine the patterns. For low concentrations, we switch from vertical to curved fingers, then ripples and finally homogeneous biofilms as the ratio of the shear to the biofilm cohesion increases. As the concentration grows, the transition between these regimes occurs at larger ratios. We usually end up with a mixture of bacterial towers infiltrated with networks of channels, unless the concentration is too large and bacteria fill all the available space. Adhesion of floating cells may change the pattern regimes. Low adhesion rates may produce patchy biofilms whereas large adhesion rates may generate wavy biofilm layers, depending

34

on erosion and growth. One must keep in mind that biofilm evolution depends on how many mechanisms are relevant in the time scale we are woking in, and what all the values of the main controlling parameters.

VI.   CONCLUSIONS

A stochastic model for submerged biofilm growth on rugose surfaces is proposed. Cell behavior is governed by a set of probabilistic rules for cell division, spreading, EPS generation, cell detachment, cell deactivation and adhesion. Different patterns are generated as a result of the collective behavior of cells acting according to the rules. Insight on the interplay of the competing mechanisms considered is gained.   Combinations of mechanisms producing patterns similar to structures observed in real biofilms are identified. The proposed framework for studying the behavior of cell aggregates is quite flexible, and may be used to test mechanisms for cell behavior or be combined with more refined descriptions of biofilm evolution. The parametric study we have performed reproduces some qualitative trends already observed in other groups experiments [36, 39–43] and in our own experiments.   Our model does not account yet for mechanical processes like cell displacement within the biofilm or movement of biofilm blocks due to external forces, which are thought to be relevant in the formation of real biofilm streamers. Further work on this issue is needed to assess its effect on the observed patterns.

In absence of floating cells, the evolution of a biofilm seed depends on a main set of parameters: the ratio of uptake rates to diffusional supply, the ratio of the shear due to the flow to the biofilm cohesion, the thickness of the concentration boundary layer and the values of the concentrations in the outer fluid.   Erosion and growth mechanisms alone are able to generate biofilm structures moving downstream. When the nutrient type and the bacterial species are fixed, different patterns are generated as the shear due to the flow or the concentration of oxygen and nutrients inside the flow vary: networks of ramified towers separated by fluid channels, vertical fingers, streamer-like structures, ripple-like patterns traveling downstream, flat biofilms, and so on. For slow or static flows, fingering is avoided when the limiting concentration reaches easily all biofilm cells. Erosion affects the growth of fingers: they may deviate in the direction of the flow or their heights may be severely reduced. Thickening flat biofilms may be eroded and kept thin. Strong erosion does not require large

flows. Small biofilm cohesion is enough. For most nutrients, increasing the ratio of the shear due to the flow to the biofilm cohesion we find more homogeneous and thinner biofilms, that may be eventually washed out, depending on the concentration. Surface roughness of the same order of magnitude as the bacterial size may anchor the biofilm and promote its survival and expansion. Other types of roughness may hinder biofilm growth. Adhesion of floating cells can change qualitatively the nature of the observed patterns. For small adhesion rates, patchy biofilms may be formed on clean surfaces. For larger adhesion rates, wavy uniform covers may appear, depending on the remaining parameters.

The insight gained on the influence of different variables in the evolution of biofilms may be useful to control their structure, either to destroy them or to use them to our advantage in different technological, medical and environmental problems.

[1] R.D. Monds and G.A. O'Toole, Trends Microbiol., 17, 73 (2009).

[2] *Research on microbial biofilms*, NIH, National Heart, Lung and Blood Institute, 2002, Tech. Rep. PA-03-047.

[3] D. Davies, Nat. Rev. Drug. Discov., 2, 114 (2003).

[4] B. Schachter, Nat. Biotechnol., 21, 361 (2003).

[5] C.M. Manuel, O.C. Nunes, and L.F. Melo, Wat. Res., 41, 551 (2007).

[6] Chien-Jung Tien, Wen-Hua Wu, Tzu-Liang Chuang, Colin S Chen, Chemosphere, 76, 1288 (2009).

[7] S. Morina, S. Pesceb, A. Tlilib, M. Costea, B. Montuelle, Ecol. Indicat., 10(2), 419 (2010).

[8] A. de las Heras and V. de Lorenzo, Chapter 19, in *Handbook of Hydrocarbon and Lipid Microbiology*, edited by Ed. K.N. Timmis, (Springer-Verlag Berlin Heidelberg, 2009).

[9] A. de las Heras and V. de Lorenzo, Analyt. Bioanalyt. Chem, 400, 1093 (2011).

[10] M. Mages, M. Ovari, W. Tümpling Jr., K. Kroft, Anal. Bioanal. Chem., 378, 1095 (2004).

[11] H. Strosnider, *Whole-cell bacterial biosensors and the detection of bioavailable arsenic* (U.S. Environmental Protection Agency, 2003).

[12] D. van Swaay, Cell-Free biofilm biosensor of catheter-related urinary tract infections, built using biobricks that exploit AHL signalling pathways in biofilms, IET, UK, 2008, DOI: 10.1049/iet-tv.46.1205

[13] E. Castellón, M. Chavarría, V. de Lorenzo, M. Zayat, and D. Levy, Adv. Mater., 22, 4846 (2010).

[14] O. Wanner, H. Eberl, E. Morgenroth, D. Noguera, C. Picioreanu, B. Rittmann, and M.C.M. van Loosdrecht, *Mathematical modeling of biofilms* (IWA Publishing, London UK, 2006).

[15] E. Morgenroth, M.C.M. Van Loosdrecht, and O. Wanner, Wat. Sc. Tech., 41, 509 (2000).

[16] M.C.M. Loosdrecht, J.J. Heijnen, H. Eberl, J. Kreft, and C. Piciorenau, Antonie van Leeuwenhoek, 81, 245 (2002).

[17] I. Klapper, C. Rupp, R. Cargo, P. Purevdorj, P. Stoodley, Biotech. Bioeng. 80, 289 (2002).

[18] N.G. Cogan and R.D. Guy, HFSP J., 4, 11 (2010).

[19] J. Wilking, T. Angelini, A. Seminara, M.P. Brenner, D.A. Weitz, M.R.S. Bulletin, 36, 385 (2011).

[20] D. Duddu, S. Boradas, D. Chopp, and B. Moran, Int. J. for Num. Meth. Eng., 74, 848 (2008).

[21] A. Seminara, T.E. Angelini, J.N. Wilking, H. Vlamakis, S. Ebrahim, R. Kolter, D.A. Weitz, M.P. Brenner, PNAS, 109, 1116 (2012).

[22] C. Picioreanu, J.U. Kreft, and M.C.M. Van Loosdrecht, Appl. Env. Microbiol., 70(5), 3024 (2004).

[23] E. Alpkvist, C. Picioreanu, M.C.M. Loosdrecht, and A. Heyden, Biotechnol. Bioeng., 94, 961 (2006).

[24] N.J. Poplawski, A. Shirinifard, S. Maciej, J.A. Glazier, Math. Biosci. Eng., 5(2), 355 (2008).

[25] C Picioreanu, MCM van Loosdrecht, JJ Heijnen, Biotechnol. Bioeng., 58, 101 (1998).

[26] J.P. Eberhard, Y. Efendiev, E. Ewing, and A. Cunningham, Int. J. Mult. Comp. Eng., 4, 496 (2005).

[27] S.W. Hermanovic, Math. Biosciences, 169, 1 (2001).

[28] G. Pizarro, D. Griffeath, and D.R. Noguera, J. Environ. Eng., 127(9), 782 (2001).

[29] B. Gottenbos, H.C. van der Mei, and H.J. Busscher, Meth. Enzymol., 310, 523 (1999).

[30] S. Lecuyer, R. Rusconi, Y. Shen, A. Forsyth, H. Vlamakis, R. Kolter, H.A. Stone, Biophys. J., 100, 314 (2011).

[31] K. Anguige, J.R. King, and J.P. Ward, Math. Biosciences, 203, 240 (2006).

[32] E. Yörük, M.F. Ochs, D. German, and L. Younes, IEEE/ACS Trans. Comp. Biol. Bioinf., 8, 592 (2011).

[33] I.W. Sutherland, Trends Microbiol., 9, 222 (2001).

[34] HC Flemming, J Wigender, Nat Rev Microb 8, 623 (2010).

[35] J.B. Xavier and K.R. Foster, Proc. Natl. Acad. Sci. USA, 104, 876 (2007).

[36] B. Purevdorj-Gage, *Pseudomonas aeruginosa biofilm structure, behavior and hydrodynamics* (PhD Thesis, Montana State University, 2004).

[37] H.J. Eberl, C. Picioreanu, J.J. Heijnen, and M.C.M. van Loosdrecht, Chem. Eng. Sc., 55, 6209 (2000).

[38] C. Picioreanu, M.C.M van Loosdrecht, J.J. Heijnen, Biotechnol. Bioeng., 72(2), 205 (2001).

[39] B. Purevdorj, J.W. Costerton, P. Stoodley, Appl. Environ. Microbiol. 68(9), 4457 (2002).

[40] P. Stoodley, I. Dodds, J.D. Boyle, and H.M. Lappin-Scott, J. Appl. Microb. Symposium. Supplement, 85, 19S (1999).

[41] P. Stoodley, Z. Lewandowski, J.D. Boyle, H.M. Lappin-Scott, Env Microb 1(5), 447 (1999).

[42] B.C. Dunsmore, A. Jacobsen, L. Hall-Stoodley, C.J. Bass, H.M. Lappin-Scott, P. Stoodley, J. Ind. Microb. Biotech. 29, 347 (2002).

[43] P. Stoodley, R. Cargo, C.J. Rupp, S. Wilson, I. Klapper, J. Ind. Microb. Biotech 29, 361 (2002).

[44] D. Rodriguez, E. Martinez, V. de Lorenzo, A. Carpio, Study of biofilm development in an industrial set up under different hydrodynamic conditions, unpublished, 2012

[45] J.W. Costerton, G.G. Geesey, and G.K. Cheng, Sci. Am., 238, 86 (1978).

[46] H. Liu, H.H.P. Fang, J. Biotechnol., 95, 249 (2002).

[47] J.W. Costerton, Int. J. Antimicrob. Agents, 11, 217 (1999).

[48] R.M. Donlan and J.W. Costerton, Clin. Microbiol. Rev., 15, 167 (2002).

[49] L. Hall-Stoodley, J.W. Costerton, P. Stoodley, Nat. Rev. Microbiol. 12, 95 (2004).

[50] L. Chai, H. Vlamakis, R. Kolter, MRS Bulletin 36, 374 (2011)

[51] I. Klapper, J. Dockery, SIAM Rev. 52, 221 (2011).

[52] T.J. Battin, W.T. Sloan, S. Kjelleberg, H. Daims, I.M. Head, T.P. Curtis, L. Eberl, Nat. Rev. Microbiol. 5, 76, (2007).

[53] M. Ghannoum, G.A. O'Toole, *Microbial biofilms* (ASM Press 2004).

[54] J.D. Bryers in *Physiological Models in microbiology*, edited by Bazin and Prosser (CRC Press, Boca Raton, 1998).

[55] R. Rusconi, S. Lecuyer, L. Guglielmini, H.A. Stone, J.R. Soc. Interface, 7, 1293 (2010).

[56] The size a of one bacterium is of order $1\mu m$. In square channels whose section is of order $b = 1\, mm$-$100\mu m$ and have steps of size a, a itself is a reasonable choice as spatial step to discretize the reaction diffusion-equations governing the concentrations or the Navier-Stokes equations for the external flow.

[57] J.C. Kissel, P.L. McCarthy, R.L. Street, J. Env. Eng. 110 (2), 393 (1984).

[58] D. De Beer, P. Stoodley, Z. Lewandowski, Wat. Res. 30 (11), 2761 (1996).

[59] T.C. Zhang, P.L. Bishop, Water Res. 28, 2267 (1994).

[60] S. Yang, Z. Lewandowski, Biotechnol. Bioeng. 48, 737 (1995).

[61] P. Stoodley, Z. Lewandowski, J.D. Boyle, H.M. Lappin-Scott, Biotech. Bioeng. 65, 83 (1999).

[62] D. de Beer, P. Stoodley, Z. Lewandowski, Biotech. Bioeng. 44, 636 (1994).

[63] P.L. Garcia-Ybarra, Phys. Rev. E 79, 067302 (2009).

[64] F.M. White, *Viscous fluid flow*, Mc Graw Hill Mechanical Engineering, 2005

[65] W.L. McCabe, J.C. Smith, *Unit operations of chemical engineering*, Chemical engineering series, New York, Mc Graw-Hill, 1976

[66] C. Picioreanu, MCM van Loosdrecht, JJ Heijnen, Biotechnol. Bioeng. 58, 101 (1998)